

On the Structure of the Orion A Cloud and the Formation of the Orion Nebula Cluster

Lee Hartmann¹ and Andreas Burkert²

lhartm@umich.edu, burkert@usm.uni-muenchen.de

ABSTRACT

We suggest that the Orion A cloud is gravitationally collapsing on large scales, and is producing the Orion Nebula Cluster due to the focusing effects of gravity acting within a finite cloud geometry. In support of this suggestion, we show how an elliptical rotating sheet of gas with a modest density gradient along the major axis can collapse to produce a structure qualitatively resembling Orion A, with a fan-shaped structure at one end, ridges or filaments along the fan, and a narrow curved filament at the other end reminiscent of the famous integral-shaped filament. The model produces a local concentration of mass within the narrow filament which in principle could form a dense cluster of stars like that of the Orion Nebula. We suggest that global gravitational contraction might be a more common feature of molecular clouds than previously recognized, and that the formation of star clusters is a dynamic process resulting from the focusing effects of gravity acting upon the geometry of finite clouds.

Subject headings: ISM: clouds, ISM: structure, stars: formation, open clusters and associations: individual (Orion Nebula Cluster)

1. Introduction

The dynamical state of molecular clouds clearly plays an important role in star formation. Older concepts of long-lived clouds, maintained in rough equilibrium by balancing turbulence and magnetic forces against gravity, are being challenged by theoretical results suggesting rapid dissipation of magnetohydrodynamic turbulence which could lead to collapse (e.g. Mac Low et al. 1998; Stone, Ostriker, & Gammie 1998; Ostriker, Gammie, &

¹Dept. of Astronomy, University of Michigan, 500 Church Street, Ann Arbor, MI 48109

²University Observatory Munich, Scheinerstrasse 1, D-81679 Munich, Germany

Stone 1999) as well as observational constraints from stellar populations which indicate short cloud lifetimes (Ballesteros-Paredes, Hartmann, & Vazquez-Semadeni 1999; Elmegreen 2000; Hartmann, Ballesteros-Paredes, & Bergin 2001; see Ballesteros-Paredes et al. 2006 and Burkert 2006 for a recent reviews). In addition, we recently pointed out the difficulties in setting up a velocity field which would globally stabilize a finite cloud containing many Jeans masses against its self-gravity (Burkert & Hartmann 2004; BH04); our results suggested that molecular clouds of appreciable mass are likely to be collapsing, at least in some regions. These developments suggest that star-forming molecular clouds are relatively transient, rapidly evolving objects.

The dynamics of molecular clouds are also likely to be highly relevant to the formation of clusters, in which most newly-formed stars reside (e.g., Lada & Lada 2003). A number of dynamical simulations of star formation have been carried out (e.g., Klessen & Burkert 2000, 2001; Bate, Bonnell, & Bromm 2002, 2003), with some semi-analytic investigations (e.g., Krumholz, McKee, & Klein 2005), but the processes responsible for assembling the protocluster gas have been given much less attention; for example, in the numerical work of Bonnell, Bate, & Vine (2003), the protocluster aggregation of gas is simply assumed as an initial condition. In BH04 we suggested that the assemblage of protocluster gas might be due to the focusing effects of gravity in finite, collapsing clouds.

The Orion A molecular cloud is a favorable site for studying the relationship between cloud dynamics and cluster formation, as it contains the Orion Nebula Cluster (ONC), the closest, relatively populous ($\gtrsim 2000$ members) young cluster containing relatively massive (O, early B) stars. In BH04 we presented an extremely simplified model of the gravitational collapse of an elliptical sheet which exhibited features in rough qualitative agreement with the structure of the Orion A cloud, forming a mass concentration near one end of the cloud which might represent the accumulation of gas for a large cluster like the ONC. In this paper we present a modified model of sheet collapse which exhibits a remarkable similarity to the structural features of the Orion A cloud. This picture makes predictions for the expected proper motions of the stellar members and suggests new perspectives both on the nature of "turbulence" in the region and on the conditions under which star clusters form.

2. Orion A and the ONC

A huge literature has been devoted to Orion A and the ONC (see Genzel & Stutzki 1989, O'Dell 2001, and references therein). Here we review the large scale morphology and kinematics of the dense gas in the cloud and the spatial relationship to the ONC.

Figure 1 shows the large-scale ^{13}CO brightness map of the Orion A cloud from Bally et al. (1987). The left panel shows the total surface brightness map, with the well-known narrowing of the cloud proceeding from south to north in roughly a “V”, culminating in the famous integral-shaped filament at the northern end. The ONC resides near the middle of the integral-shaped filament (see below).

The right panel of Figure 1 shows the radial velocity distribution of the ^{13}CO emission summed over right ascension as a function of declination. Here we call attention to features already discussed by Kutner et al. (1977), Bally et al. (1987), Maddalena et al. (1986), and Heyer et al. (1992) but which deserve particular emphasis. First, there is the well-known overall radial velocity gradient from south to north, with a velocity difference of $\sim 8 \text{ km s}^{-1}$ from one end to the other (see also Wilson et al. 2005). If we take the total mass of the Orion A cloud to be $1.1 \times 10^5 M_{\odot}$ from Wilson et al. (2005), and a half-cloud length R of 2.5 degrees $\sim 16 \text{ pc}$ at a distance of 470 pc, then a characteristic virial velocity is $(GM/R)^{1/2} = 4.9 \text{ km s}^{-1}$. Thus, the observed $\sim \pm 4 \text{ km s}^{-1}$ systematic velocity gradient along the cloud is dynamically significant (Kutner et al. 1977; Bally et al. 1987).

The second general feature worth noting in the right panel of Figure 1 is that the velocity distribution shows many coherent structures (e.g., Bally et al. 1987). Significant lumps of gas with distinct kinematics can be seen all along the cloud, with velocity differences of roughly $2 - 3 \text{ km s}^{-1}$. Heyer et al. (1992) found that some of these structures appear to be bubbles in ^{12}CO , and suggested that they might be wind-driven. There is a particularly large velocity systematic gradient at the northern end of the cloud running from a velocity of 11 km s^{-1} to about $7 - 8 \text{ km s}^{-1}$ proceeding southward, corresponding to the integral-shaped filament (see also Wilson et al. 2005). There is also evidence for an especially large local velocity dispersion at a declination of $\sim -5.4^{\circ}$ (1950), which is near the center of the ONC.

To illustrate the spatial distribution of the young stars in and near the ONC we use infrared-detected stars selected from the systematic survey of Carpenter, Hillenbrand, & Skrutskie (2001) from deep scans using the 2MASS telescope. Although it is impossible to exclude non-members completely from this data, it is useful for our limited purposes because it is not optically-biased (although extinction can still have some effect) and has relatively uniform sensitivity over a wide area. To limit the contamination by non-members, we used the pre-main sequence tracks in the K vs. $H - K$ diagram as developed by Hillenbrand & Carpenter (2000) for a 1 Myr-old population at 480 pc. Following this prescription, we included all stars with $K_s \leq 10.5$, plus all stars with $10.5 < K_s \leq 12.5$ and $H - K_s \geq 0.4 + 0.1(K_s - 13.0)$. These selection criteria probably do not remove all non-members but yield a relatively unbiased, large-scale view of the stellar population.

In Figure 2 we show a closer view of the ONC region. The right panel shows the spatial

distribution of the infrared sources as selected above; this is very similar to that found by Carpenter et al. (2001) for infrared variables (likely pre-main sequence members), though this selection resulted in fewer stars given photometric uncertainties and small amplitudes of variability in the near-infrared. The middle panel shows the stellar distribution superimposed upon the total ^{13}CO emission, while the left panel shows the position-velocity diagram in ^{13}CO over the same right ascension range as shown in the other panels.

As Figure 2 shows, the ONC is characterized by a dense, oval concentration of stars with a length (in the long dimension) of about 0.2 degree ~ 1.6 pc at a distance of 470 pc. Beyond this, the extended distribution becomes much more filamentary. The elongated main body of stars appears to have a somewhat different position angle on the sky than the extended filament. These features had been recognized and characterized quantitatively by HH98. Fitting the stellar surface densities (optical and infrared sources) with ellipses, HH98 found an ellipticity of roughly 0.3 on scales (semi-major axes) less than 216 arcsec ~ 0.5 pc to 0.5 on a scale (semi-major axis) of 532 arcsec ~ 1.2 pc. They also found evidence for a slight shift in position angle of the major axis from slightly west of north on small scales to slightly east of north on the largest scale considered. These features appear consistent with recent Spitzer imaging (S.T. Megeath, personal communication). The larger scale view provided by the Carpenter et al. (2001) sources suggests that it might be better to view the ONC as a dense, moderately elongated core embedded in a larger-scale filamentary stellar distribution rather than an object having a smoothly-varying ellipticity as a function of radius.

Figure 2 shows that the gas exhibits spatially-coherent kinematic structure in the vicinity of the ONC. In particular, as noted above, there is clearly a larger velocity dispersion in the gas near the ONC center. Moreover, there are distinct velocity systems within ± 0.2 degrees of the ONC center ($\sim \pm 1.6$ pc at a distance of 470 pc), with a distinct hook-shaped pattern in the northern arm of the filament with a high velocity gradient running from about 11 km s^{-1} at DEC ~ -5 to about $7 - 8 \text{ km s}^{-1}$ at DEC ~ -5.5 (Bally et al. 1987; Wilson et al. 2005). This behavior may suggest gravitational acceleration toward the cluster center (see §5.2). We will discuss the implications of this structure in greater detail in a subsequent paper which will include stellar radial velocities (Furesz et al. 2006).

In addition to the concentration of stars near the dense filament, there is also a spatially-extended population of potential members. Many of these objects are likely to be associated pre-main sequence stars. Rebull et al. (2000) performed optical photometry of the fields around the main concentration of the ONC, and demonstrated that many of these stars are pre-main sequence members with ages $\log(t/\text{yrs}) = 6.0 \pm 0.4$, consistent with but possibly a bit older than the stars in the central Trapezium region studied by Hillenbrand (1997). Moreover, Rebull et al. showed that many of these stars have ultraviolet excesses consistent

with disk accretion. In addition, the results of both Carpenter et al. (2001) and the extended Spitzer Space Telescope study of the region (S.T. Megeath, personal communication) show that there are significant numbers of objects with disk-like infrared excess emission. Thus, the story of star formation in the region must include a consideration of the distributed population as well as that of the “cluster” stars.

The significant kinematic substructure in the Orion A cloud, the large velocity gradients and dispersions in the gas near the ONC, and the clear extension of the ONC along the dense filament all suggest that a dynamical model might be appropriate for understanding the observed structure. The overall velocity gradient in the cloud suggests that rotation might be an important factor (Kutner et al. 1977). In the following section we construct an extremely simple rotating cloud model which highlights the potential role of gravity in dynamically producing a roughly similar structure.

3. Model

To demonstrate how gravitational collapse might explain the morphology of Orion A and produce a potential protocluster gas concentration, we construct a simple two-dimensional, self-gravitating sheet model similar to those in BH04. The choice of sheet geometry is motivated by a desire to construct an initial simple model with as few free parameters as possible. It is also consistent with our proposal that local molecular clouds are formed by material swept up by large-scale flows (Ballesteros-Paredes, Hartmann, & Vazquez-Semadeni 1999; Hartmann, Ballesteros-Paredes, & Bergin 2001 = HBB01; Bergin et al. 2004; BH04).

BH04 showed that an initially elongated cloud will tend to collapse to a more filamentary distribution, with a tendency to form high-density regions near the ends of the cloud, and argued that many regions (such as Orion) showed a tendency to have clusters form near the ends of the clouds. BH04 also showed that an elliptical sheet with a smooth surface density gradient along the major axis would produce a “V-shaped” cloud with a mass concentration (potential protocluster gas) at the apex of the “V”, qualitatively similar to what is observed in Orion A. We now introduce a few refinements to this simple model to produce an even closer resemblance to observations.

As in BH04, the numerical calculations are performed on a two-dimensional Eulerian, Cartesian grid. The full computational region with dimension $2 \times L$ is represented by a grid, composed of $N \times N$ grid cells, equally spaced in both directions. Under the assumption of isothermality, the relevant differential equations to be integrated are the hydrodynamical continuity and momentum equations:

$$\begin{aligned}\frac{\partial \Sigma}{\partial t} + \vec{\nabla} \cdot (\Sigma \vec{v}) &= 0 \\ \frac{\partial \vec{v}}{\partial t} + (\vec{v} \cdot \vec{\nabla}) \vec{v} &= -\frac{\vec{\nabla} P}{\Sigma} - \vec{\nabla} \Phi\end{aligned}\tag{1}$$

where $\Sigma(\vec{x})$, $P(\vec{x})$ and $\vec{v}(\vec{x})$ are the gas surface density, pressure and two-dimensional velocity vector at position \vec{x} , respectively. The gravitational potential Φ is determined, solving Poisson's equation in the equatorial plane (Binney & Tremaine 1987)

$$\nabla^2 \Phi = 4\pi G \Sigma\tag{2}$$

with G the gravitational constant. The isothermal equation of state

$$P = c_s^2 \Sigma\tag{3}$$

determines the pressure for a given surface density Σ and sound speed c_s .

This set of equations is integrated numerically by means of an explicit finite second-order van Leer difference scheme including operator splitting and monotonic transport as tested and described in details in Burkert & Bodenheimer (1993,1996). In order to suppress numerical instabilities, an artificial viscosity of the type described by Colella & Woodward (1984) is added (Burkert et al. 1997).

The Poisson equation is integrated on the grid under the assumption that there is no matter outside of the computational region. As we are focusing here on the gravitationally unstable sheets that collapse towards the center of the region, outflow of gas beyond the outer boundaries can be neglected. Therefore the outflow velocities at the outer boundary are set to zero and a negligible pressure gradient is assumed. Most calculations were typically performed with 256^2 grid cells of size $\Delta = 2L/N$, where $2L$ is the largest dimension of the rectangular computational region. Test calculations with $N=128$ and $N=512$ did not result in significant differences. In these calculations the code units were set such that $G = 1$. In this paper we will focus on our favorite model with the following density distribution in code units:

$$\begin{aligned}\Sigma(R) &= \Sigma_0 \times g(x) \text{ for } R \leq 0.5L; \\ \Sigma(R) &= \Sigma_0 \times g(x) \exp\left(-\frac{(R/L - 0.5)^2}{0.09}\right)\end{aligned}\tag{4}$$

$$\begin{aligned} & \text{for } 0.5L \leq R \leq 0.8L; \\ \Sigma(R) &= 10^{-3}\Sigma_0 \text{ for } R > L. \end{aligned}$$

with

$$g(x) = 0.065 + 2.17 \frac{x - L}{2L} \quad (5)$$

and

$$R \equiv (x^2 + \epsilon^2 y^2). \quad (6)$$

Here $\epsilon = 0.4$ is the initial ellipticity of the sheet. We adopted a long axis of $L=0.8$ and a surface density $\Sigma_0 = 1.125$ which gives to a total mass of $M = 1$. Finally, we introduced some initial solid-body rotation,

$$\begin{aligned} v_x(x, y) &= -\Omega y \\ v_y(x, y) &= \Omega x. \end{aligned} \quad (7)$$

with $\Omega = 2.5$ for this particular model. The sound speed was set to $c_s = 0.1$ which makes the sheet highly Jeans unstable.

The upper left panel of Figure 3 is a snapshot at a very early time and thus illustrates essentially the initial surface density distribution. Basically, the initial model is an elliptical sheet with an overall smooth surface density gradient running in the direction of the major axis and a turndown of the surface density near the edge of the sheet.

Figures 3 and 4 show the time evolution of the model. The overall density gradient produces denser structures at one end of the cloud, which collapse faster and eventually result in a narrow filament. At the wider, lower-density end of the cloud, the collapse produces two ridges in the form of a “V” shape, resulting from the non-linear gravitational acceleration that naturally occurs in finite sheets (BH04). The rotation of the cloud leads to a twist of the narrow filament relative to the “V-shaped” lower cloud (last panels in Figure 4), and to the development of curvature in the filament reminiscent of the integral-shaped filament. If there were no rotation in our model, the assumed initial conditions would result in a straight filament aligned along the symmetry axis of the V-shaped cloud, with no integral-shaped filament.

Dense lumps of gas are produced in the filament, which could represent the collection of protocluster gas that could collapse and fragment into a star cluster. BH04 already showed the propensity of collapse of elongated sheets to produce dense gas concentrations near the ends of filaments; we regard this as a general result, although the details of this fragmentation (number, mass, size) are unreliable due to limited resolution. The turndown of density at the edge of the original sheet results in the dense concentrations of gas lying inside of the end of the filamentary gas, rather than right at the end of the filament as in BH04. The relatively large rotation of the cloud and the gravitational acceleration toward the narrow end prevent the lower part of the cloud from collapsing significantly.

The simulation does not develop small fragments that might form individual subclusters (our resolution is far too low to examine individual star formation). As we found in BH04, local linear perturbations greater than a Jeans mass do not grow faster than the overall collapse of a sheet. There must be non-linear, small-scale perturbations for stars to fragment out of this sheet, as might be produced initially through instabilities a cloud-forming shock front (e.g., Audit & Hennebelle 2005; Heitsch et al. 2005, 2006; Vazquez-Semadeni et al. 2006).

Figure 5 shows position-velocity diagrams along the x and y axes for the final configuration that corresponds to the lower panels of Figure 4. The position-velocity distributions have been smoothed with a top-hat filter of width $\Delta x, y = 0.025$ and $\Delta v = 0.5$. The left panel shows the logarithm of the gas mass that moves with y-velocity v_y at position x. The two kinematically distinct ridges of mass for $x < 0$, corresponding to the infall from either side of the collapsing sheet. For $0 \lesssim x \lesssim 0.25$ a third ridge is present which is the result of infall within the central regions of the sheet toward the apex of the V. For $0.3 \lesssim x \lesssim 0.4$ complex kinematic structure arises with a very large velocity dispersion. This is a result of the gravitational acceleration of gas in the region of influence of the dense gas lumps. The details of this structure and the exact magnitude of these velocities must be regarded as uncertain because of the limited resolution of the model.

The right panel of Figure 5 shows somewhat similar behavior, except that the infall in the lower part of the cloud has only a small component in the x direction and therefore the two ridges of emission do not appear.

4. Comparison with Orion A

Figure 6 shows a side-by-side comparison of the Orion A spatial distribution of ^{13}CO emission from Figure 1. The model has been scaled so that one code unit of distance is

~ 40 pc, a value we use in the discussion of kinematics (see below). The qualitative resemblance of the model to the observations is clear; the cloud narrows from an approximately “V-shaped” structure to an integral-shaped filament with one dense clump and a lower density clump near the equivalent position of the ONC in Orion A. Interestingly, *Spitzer Space Telescope* observations of the lower Orion A cloud provide evidence for an enhanced population of young stars in the north-east ridge of the “V” (S.T. Megeath, personal communication), which suggests that, as in the model, this structure really is one of high density rather than simply high line-of-sight emission.

The model is clearly not a perfect reproduction of the Orion A cloud, which has additional complex structure. For example, the southwest ridge of Orion A does not seem to be as dense as in this model. Putting in lower densities in the bottom half of the initial ellipse would presumably improve the agreement with observations, but the present simple model suffices to illustrate the general idea. In addition, the upper part of the integral-shaped filament may not contain sufficient mass in comparison with the real object. This may be due in part to resolution effects, or simply that we need a somewhat different initial density distribution. There is also more extended, lower-density gas seen in ^{12}CO which the model does not address; this would presumably require an initially more extended, low-density envelope.

As the motions are generated by gravity in a cloud with angular momentum, kinematics can provide an important test of the model. However, it is difficult to make direct test for this two-dimensional model, as we do not know the inclination to the line of sight and the real object is three-dimensional. Nevertheless, we calculate scaled velocities to provide some indication of what might be observed.

The code unit of velocity corresponds to physical units

$$v(\text{unit}) = (GM(\text{unit})/(R(\text{unit})))^{1/2}, \quad (8)$$

where $M(\text{unit})$ is the physical mass that corresponds to 1 code mass unit and $R(\text{unit})$ is the physical length that corresponds to one code length unit. We are basically modelling what Wilson et al. (2005) called “region 2” in the Orion A cloud, which ranges from galactic longitudes of 208° to 213° at a galactic latitude $\sim -20^\circ$; hence we take the total length of the cloud to be $5^\circ \times \cos(20) \sim 39$ pc at a distance of 470 pc. Wilson et al. (2005) give the total mass in region 2 as $M = 7 \times 10^4 M_\odot$. At the end of our simulation the region that corresponds to region 2 has a length of ~ 1 code units and contains a total mass of order 0.6 mass units. Thus a length unit corresponds to $R(\text{unit}) \approx 39$ pc and a mass unit to $M(\text{unit}) \approx 1.1 \times 10^5 M_\odot$ (which is approximately the total Orion A cloud mass estimated by Wilson et al. 2005). Then the velocity code unit becomes $v(\text{unit}) \sim 3.5 \text{ km s}^{-1}$.

Applying this scaling to Figure 5, we find the following results. In the left panel (velocities in the y-direction), the “filaments” at $x < 0.2$ are spaced by approximately 1.5 to 2 code units, or $\sim 5 - 7 \text{ km s}^{-1}$. The “middle filament” in position-velocity space has an overall velocity shift from $-0.5 < x < 0.2$ of slightly less than 2 units, or about 6 km s^{-1} . The observed values of occasional velocity splitting and overall velocity gradient (right panel of Figure 1) are about 1/2 to 2/3 as large as these values, so the agreement is reasonable, especially considering possible projection effects; even ignoring the inclination of the sheet to the line of sight, the velocities in the x-direction (right panel) are much smaller than observed, because of the strongly anisotropic nature of the velocity field. We also note that some of the velocity splitting in Orion A may be due to stellar-wind driven bubbles (see §5.5) which is not part of this simple model.

The model velocity dispersions near the apex of the V and the filament are much larger than the radial velocity dispersions observed in the similar regions in Orion A. At $x \sim 0.25$, the velocity width in the left panel is about 4 units, or $\sim 14 \text{ km s}^{-1}$, while the radial velocity width of the ^{13}CO emission is closer to 4 km s^{-1} . Again, the x velocity shows very little velocity dispersion. This might indicate an additional tilt of the gas structure of Orion A in the third (z) direction that cannot be modeled by our 2-dimensional simulations. Both projections show very large velocity dispersions near the dense concentration(s) in the integral-shaped filament, of order 6 code units or $\sim 20 \text{ km s}^{-1}$ that are much larger than observed. However, it should be emphasized that near the tip of the V and the filament the results are uncertain because of limited resolution, which could have a major effect on the calculated velocities. As indicators of this, the separate “blobs” in position-velocity space seen in Figure 5 represent just a few grid cells each at most. In addition, we note that the maximum velocities in the computation essentially double from the second-last snapshot at $t = 0.209$ to $t = 0.25$, suggesting great sensitivity to the chosen time of comparison - probably also a reflection of limited resolution. Finally, the gravitational potential of the stars in the ONC should also be taken into account in an improved model.

The rotational motion making the integral-shaped filament is especially apparent in the x-velocity (right panel of Figure 5), where the generally positive velocity components quickly reverse to negative velocities at $x > 0.25$. This raises the question as to whether the hook-shaped velocity structure in the northern half of the real filament (Figure 2) might be a signature of the rotational motion, accelerated by gravitational collapse. To be consistent with the model, one would have to assume that the plane of the initial sheet was tilted so that its western side is closer to Earth.

We conclude that our model velocities are at least consistent with observed gas radial velocities in the sense that they can be as large or larger than observed. It is difficult to

say more than this, given the unknown projection effects and the uncertainty in the velocity field near the poorly-resolved densest regions. Higher-resolution, 3-dimensional simulations are required to explore this issue further.

5. Discussion

We have shown that a gravitationally-collapsing cloud with smooth, simple properties can evolve into a more complex structure qualitatively similar to that of Orion A (Figure 6). Although our specific model parameters are not unique, the general requirements are plausible:

(1) The initial molecular cloud was elongated. Flow-produced clouds will naturally tend to be flattened, and the general case would be for one lateral dimension to be longer than the other.

(2) The initial internal velocities were sufficiently small to allow collapse, or they dissipated sufficiently quickly to allow collapse.

(3) The cloud was formed with angular momentum.

(4) The elongated cloud initially had more mass at one end than the other and had a turndown of density near its edge.

Our model provides a natural explanation for the formation of the narrow integral-shaped filament without requiring specific focusing flows driven by an unknown mechanism. The condensations which we find the S-shaped filament could form a cluster of stars like the ONC. The large velocity gradient observed in this region in our simulations results from gravitationally accelerated gas when falling into the deep potential well generated by the condensation, coupled with rotation. The collapse model is dynamically plausible; all that is required is to assume that the stellar energy input, particularly that of the central O star has not yet disrupted the dense gas. In contrast, equilibrium or quasi-equilibrium models must explain how to support a very massive filament against its self-gravity and how to maintain the observed massive, supersonically-moving clumps of gas without either overshooting (blowing the region apart) or undershooting (gravitational collapse, as in our picture).

The model predicts that there should be some measurable rotation in the plane of the sky; although the model velocities are uncertain in this region, they could easily be several km s^{-1} . The proper motions of stars in the ONC should reflect this motion to some extent, particularly the stars at either end where the cluster is most filamentary. Unfortunately,

the methods used by Jones & Walker (1988) to measure proper motions were such as to eliminate any effect of rotation (or expansion; e.g., Scally, Clarke, & McCaughrean 2005). Future proper motion measurements should provide a direct test of the model.

5.1. Ages and structure

Another perhaps initially surprising feature of this model is the rapidity of the collapse. The physical time of the code time units is $(R^3/GM)^{1/2}$, which, for the parameters adopted in §4, is $t(\text{unit}) = 6.7$ Myr. Thus, the time taken for the collapse of the original ellipse, with an initial semi-major axis of 24 pc and a semi-minor axis of 4.8 pc, is only 1.7 Myr. Obviously this is not a very precise estimate, as it depends crucially on just what the original form of the cloud was, and perhaps on the timescale of dissipation of local turbulence, but it is clearly consistent with the typical estimated ages of 1-3 Myr for stars in the region (Hillenbrand 1997; Rebull et al. 2000).

As shown in the right-hand panel of Figure 1, there are clearly lumps of gas correlated in space and in velocity; these regions cannot have experienced more than about one crossing or collapse time; otherwise the velocity structure would be erased as the infalling gas shocks and dissipates its kinetic energy. The stars would tend to pass through the shocked gas, reducing the spatial correlation of stars with dense gas. All of these features suggest that Orion A is dynamically young, in agreement with our model.

5.2. Dynamics and Formation of the ONC

Our model suggests that the gas for the ONC was assembled by large-scale gravitational collapse. In contrast, Tan, Krumholz, & McKee (2006; TKM06) have argued for a picture in which rich star clusters take several dynamical times to form, are quasi-equilibrium structures during formation, and thus initial conditions are not very important. In particular, TKM06 discuss the ONC and argue that it is several crossing times old, and argue that its smooth structure supports their quasi-equilibrium picture (see also Scally & Clarke 2002). However, it is difficult to see how to maintain an equilibrium condition in a system with many thermal Jeans masses, rapidly dissipating turbulence, and the destructive effects of stellar energy input; as Bonnell & Bate (2006) argue, it is much easier to undershoot or overshoot than maintain a balance.

In a subsequent paper (Furesz et al. 2006) we will discuss evidence from the stellar kinematics suggesting that the ONC is not in a dynamical equilibrium. Here we simply

make two points. First, the spatially-coherent kinematic substructure seen in the vicinity of the ONC (Figures 1 and 2) does not obviously suggest equilibrium conditions; the large velocity gradient in the northern end of the integral-shaped filament might be produced by infalling gravitationally-accelerated gas (which would not be surprising, as the mass of the stars in the cluster provides additional acceleration toward the center. Second, the stellar distribution is clearly filamentary on radial scales $r \gtrsim 1$ pc, not typical of a relaxed system.

5.3. Bound Clusters?

Early discussions of cluster formation (e.g., Lada, Margulis, & Dearborn 1984; Mathieu 1983) assumed initial conditions such that the stars had virial kinetic energies and then considered how efficient star formation must be to end up with a bound (open) cluster. More recently, Adams (2000) studied the dependence of bound cluster formation on its anisotropy. Geyer & Burkert (2001) showed that a cluster which is already in virial equilibrium when the remaining gas is ejected will only remain gravitationally bound only if more than 50% of the gas was converted into stars. Gas expulsion from a collapsing star cluster with initially small velocity dispersion could however produce a bound cluster even for low star formation efficiencies of order 10% (see also Lada et al. 1984). In the simulations discussed by Bonnell, Bate, & Vine (2003), which assumed an initial turbulent velocity field in the gas with dispersion comparable to the virial value, the turbulence quickly dissipated as stars formed and the cluster gas began to contract gravitationally. Our model suggests that the infall motions might be even more important initially; the overall collapse of the cloud, with the consequent effect of producing a time-variable gravitational potential, could increase the importance of violent relaxation in altering the stellar distribution (e.g., Binney & Tremaine 1987). Gravitational collapse produces velocities only $2^{1/2}$ times larger than virial values, and it is still quite possible that a bound remnant cluster can result with even modest efficiencies of star formation depending upon the details of the stellar spatial and velocity distributions (e.g., Boily & Kroupa 2003). Addressing these issues further will require more sophisticated simulations including stars as well as gas.

5.4. Cloud dynamics

The collapse picture naturally produces large-scale velocity gradients of “virial” magnitude, as seen in the north-south gradient in Orion A; approximate agreement between kinematic and gravitational terms as inferred from the virial theorem is obviously not a good indicator of true virial equilibrium (Ballesteros-Paredes 2006). Given an initial cloud

angular momentum, collapse might also naturally result in large scale rotation near centrifugal balance, as suggested by the radial velocity gradient observed in Orion A. This model also suggests that a significant fraction of the “turbulence” could be gravitationally-generated. Stellar energy input such as outflows, photoionization, and winds will certainly produce additional turbulence, especially in the low-density regions; but gravity should be much more efficient in accelerating large, dense lumps of gas and stars. Indeed, as BH04 pointed out, it is extremely difficult if not practically impossible to avoid generating significant gravitational “turbulence” in clouds of many thermal Jeans masses if there is any substructure to the cloud (though these motions might be called more properly gravitational flows than turbulence).

The collapse model implies that Orion A is globally magnetically supercritical; otherwise the magnetic fields would prevent collapse. A similar conclusion applying to molecular clouds in general was reached by Bertoldi & McKee (1992) on different grounds. If molecular clouds are globally supercritical, then any subcritical regions must be balanced by other, even more than average supercritical regions. The further implication is that there is in general little if any magnetic barrier to star formation, and so star formation can be “fast”, as required observationally (HBB01).

Global collapse would also make it easier to assemble molecular clouds from large-scale flows in the diffuse atomic interstellar medium in the solar neighborhood. Bergin et al. (2004) computed one-dimensional shock models with chemistry and showed that the requirement of a minimum surface density to shield the CO from the interstellar ultraviolet radiation field might imply sweep-up timescales of several to 20 Myr, depending upon the initial pre-shock density. However, if the cloud can gravitationally contract in the *lateral* direction, there can be a runaway process of increasing column density on much shorter timescales - a few Myr or less, in the case of Orion A.

5.5. Stellar energy input

If global gravitational collapse is a general feature of nearby molecular clouds, why is the local star formation rate so low? Turbulent support is ineffective in preventing collapse in dense regions (e.g., Stone, Ostriker, & Gammie 1998; Mac Low et al. 1998; Heitsch, Mac Low, & Klessen 2001) unless driven, and even then it is difficult to inject the energy into the densest fragments most in need of support (Balsara 1996; Elmegreen 1999; Heitsch et al. 2005, 2006). The high-mass stars in Orion A will almost certainly disrupt at least the northern end of the ONC; θ^1 C Ori is already photodissociating and photoionizing the filament gas at a rapid rate (O’Dell 2001), it will probably become a supernova and disrupt

much of the remaining cloud in 3-5 Myr. The efficiency of low-mass stars in blowing away material from the southern end of the cloud might be significant, though this is less certain (e.g., Matzner & McKee 2000).

The possibility that much or all of the cloud motions and structure discussed here are due to stellar energy input is difficult to reject conclusively. Bally et al. (1987) suggested that the entire cloud might be shaped by pressure from the Orion superbubble, and Wilson et al. (2005) suggested that the hook-shaped velocity structure might also be due to pressure from the stellar winds of the Orion 1b subgroup. Heyer et al. (1992) noted the presence of several bubble-like structures in ^{12}CO (see also Bally 1989) which might be driven by stellar winds. However, Heyer et al. also noted that the energetics of the observed bubbles were probably not sufficient to disrupt the L1641 (lower) cloud region. The bubbles are less apparent in the ^{13}CO map, which traces denser gas than ^{12}CO (cf. Wilson et al. 2005). Moreover, it is hard to see how the structure and the coherent streaming velocities of the extremely dense and massive integral-shaped filament can be created in this way. Indeed, it is not obvious from the ^{13}CO intensity map alone just where the ONC and the central ionizing O star reside, as one might expect if stellar energy input were dominant. Similarly, the northwest ridge or the lower region of the Orion A cloud exhibits the highest concentration of young stars (S.T. Megeath, personal communication) which is not an obvious result of driving by the lower-mass stars in this region. For these reasons we argue that driving by stellar energy input, while significant in making substructure within the cloud, is not the major influence shaping the global structure of Orion A.

6. Conclusions

We have developed a simple model of a gravitationally collapsing molecular cloud which accounts the overall morphology of the Orion A cloud and suggests the formation of a mass concentration in a location similar to that of the ONC. Further kinematic studies, especially stellar proper motions, can be used to test this picture. Our model implies that star cluster formation at least in some cases is a dynamic, complex process, with gravitational collapse playing an essential role in assembling the protocluster gas. Future simulations in three dimensions including stars as well as gas will be needed to test new and improved kinematic measurements of the stellar population, providing additional insight into the formation of the ONC.

We are grateful to Bob Wilson for providing the ^{13}CO data of Orion A, to John Carpenter for providing the stellar positions of the infrared sources found in his survey, and to Fabian

Heitsch with IDL help and comments on the manuscript.

REFERENCES

- Adams, F.C. 2000, *ApJ*, 542, 964
- Audit, E., & Hennebelle, P. 2005, *A&A*, 433, 1
- Ballesteros-Paredes, J. 2006, *astro-ph/0606071*
- Ballesteros-Paredes, J., Vázquez-Semadeni, E., & Scalo, J. 1999, *ApJ*, 515, 286
1999*ApJ*...527..285B
- Ballesteros-Paredes, J., Hartmann, L., & Vázquez-Semadeni, E. 1999, *ApJ*, 527, 285
- Ballesteros-Paredes, J., Klessen, R.S., Mac Low, M.-M., & Vazquez-Semadeni, E. 2006, in *Protostars and Planets V*, eds. B. Reipurth, D. Jewitt, & K. Keil (Tucson: University of Arizona Press), in press (*astro-ph/0603357*)
- Bally, J., in *Proc. ESO Workshop on Low-Mass Star Formation and Pre-Main Sequence Objects*, ed. B. Reipurth (Garching: ESO), 1
- Bally, J., Stark, A. A., Wilson, R. W., & Langer, W. D. 1987, *ApJ*, 312, L45
- Balsara, D. S. 1996, *ApJ*, 465, 775
- Bate, M. R., Bonnell, I. A., & Bromm, V. 2002, *MNRAS*, 332, L65
- Bate, M. R., Bonnell, I. A., & Bromm, V. 2003, *MNRAS*, 339, 577
- Bergin, E. A., Hartmann, L. W., Raymond, J. C., & Ballesteros-Paredes, J. 2004, *ApJ*, 612, 921
- Bertoldi, F., & McKee, C. F. 1992, *ApJ*, 395, 140
- Binney, J. & Tremaine, S. 1987, *Galactic Dynamics* (Princeton Univ. Press), pp 271-273
- Boily, C. M., & Kroupa, P. 2003, *MNRAS*, 338, 673
- Bonnell, I. A., Bate, M. R., & Vine, S. G. 2003, *MNRAS*, 343, 413
- Bonnell, I. A., & Bate, M. R. 2006, *MNRAS*, in press (*astro-ph/0604615*)

- Burkert, A. 2006, in *Statistical Mechanics of Non-Extensive Systems*, ed. F. Combes & R. Robert (Elsevier), astro-ph/0605088
- Burkert, A., Bate, M.R. & Bodenheimer, P. 1997, *MNRAS*, 289, 497
- Burkert, A. & Bodenheimer, P. 1993, *MNRAS*, 264, 798
- Burkert, A. & Bodenheimer, P. 1996, *MNRAS*, 280, 1190
- Burkert, A., & Hartmann, L. 2004, *ApJ*, 616, 288 (BH04)
- Carpenter, J. M., Hillenbrand, L. A., & Skrutskie, M. F. 2001, *AJ*, 121, 3160
- Collela, P. & Woodward, P. 1984, *J. Comput. Phys.* 54, 174
- Elmegreen, B. G. 2000, *ApJ*, 530, 277
- Genzel, R., & Stutzki, J. 1989, *ARA&A*, 27, 41
- Geyer, M.P., & Burkert, A. 2001, *MNRAS*, 323, 988
- Furesz, G. et al. 2006, in preparation
- Hartmann, L., Ballesteros-Paredes, J., & Bergin, E. A. 2001, *ApJ*, 562, 852 (HBB01)
- Hillenbrand, L. A. 1997, *AJ*, 113, 1733
- Hillenbrand, L. A., & Carpenter, J. M. 2000, *ApJ*, 540, 236
- Hillenbrand, L. A., & Hartmann, L. W. 1998, *ApJ*, 492, 540 (HH98)
- Heitsch, F., Burkert, A., Hartmann, L. W., Slyz, A. D., & Devriendt, J. E. G. 2005, *ApJ*, 633,
- Heitsch, F., Burkert, A., Hartmann, L. W., Slyz, A. D., & Devriendt, J. E. G. 2006, *ApJ*, in press
- Heitsch, F., Mac Low, M.-M., & Klessen, R. S. 2001, *ApJ*, 547, 280
- Heyer, M. H., Morgan, J., Schloerb, F. P., Snell, R. L., & Goldsmith, P. F. 1992, *ApJ*, 395, L99
- Jones, B. F., & Walker, M. F. 1988, *AJ*, 95, 1755
- Klessen, R. S., & Burkert, A. 2000, *ApJS*, 128, 287

- Klessen, R. S., & Burkert, A. 2001, *ApJ*, 549, 386
- Krumholz, M. R., McKee, C. F., & Klein, R. I. 2005, *Nature*, 438, 332
- Kutner, M. L., Tucker, K. D., Chin, G., & Thaddeus, P. 1977, *ApJ*, 215, 521
- Lada, C. J., & Lada, E. A. 2003, *ARA&A*, 41, 57
- Lada, C. J., Margulis, M., & Dearborn, D. 1984, *ApJ*, 285, 141
- Mac Low, M.-M., Klessen, R. S., Burkert, A., & Smith, M. D. 1998, *Physical Review Letters*, 80, 2754
- Maddalena, R. J., Morris, M., Moscowitz, J., & Thaddeus, P. 1986, *ApJ*, 303, 375
- Mathieu, R. D. 1983, *ApJ*, 267, L97
- Matzner, C. D., & McKee, C. F. 2000, *ApJ*, 545, 364
- O’Dell, C. R. 2001, *ARA&A*, 39, 99
- Ostriker, E. C., Gammie, C. F., & Stone, J. M. 1999, *ApJ*, 513, 259
- Rebull, L. M., Hillenbrand, L. A., Strom, S. E., Duncan, D. K., Patten, B. M., Pavlovsky, C. M., Makidon, R., & Adams, M. T. 2000, *AJ*, 119, 3026
- Scally, A., & Clarke, C. 2002, *MNRAS*, 334, 156
- Scally, A., Clarke, C., & McCaughrean, M. J. 2005, *MNRAS*, 358, 742
- Stone, J. M., Ostriker, E. C., & Gammie, C. F. 1998, *ApJ*, 508, L99
- Tan, J. C., Krumholz, M. R., & McKee, C. F. 2006, *ApJ*, 641, L121 (TKM06)
- Vázquez-Semadeni, E., Ryu, D., Passot, T., González, R. F., & Gazol, A. 2006, *ApJ*, 643, 245
- Wilson, B. A., Dame, T. M., Mashedier, M. R. W., & Thaddeus, P. 2005, *A&A*, 430, 523

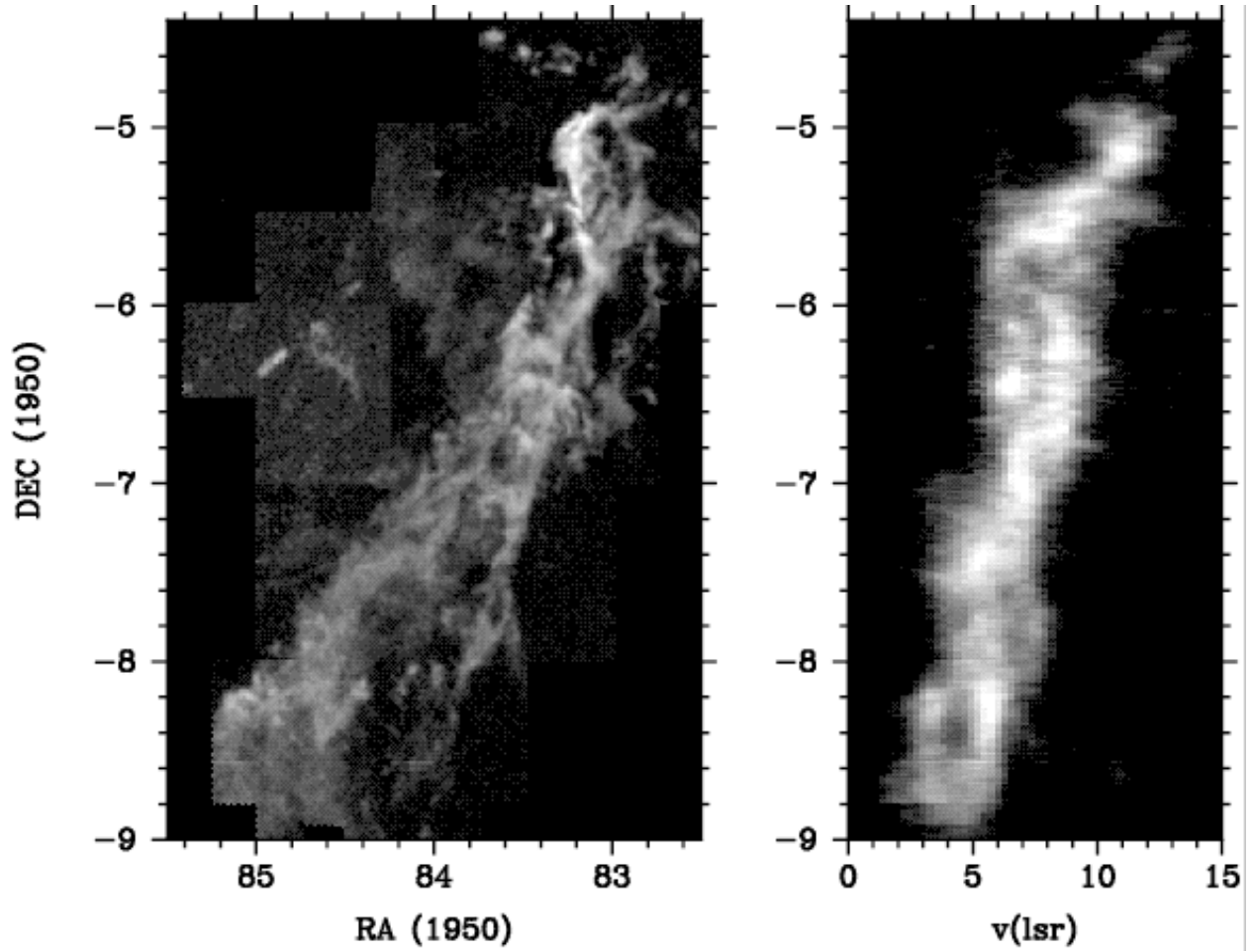


Fig. 1.— Large-scale ^{13}CO distribution in the Orion A cloud, taken from Bally et al. (1987). The left panel shows the total brightness distribution; the overall “V”-shaped nature of the cloud is apparent, with the famous “integral-shaped” filament apparent at the northern end of the cloud. The right panel shows the velocity distribution of the ^{13}CO emission, summed over right ascension, as a function of declination (see text)

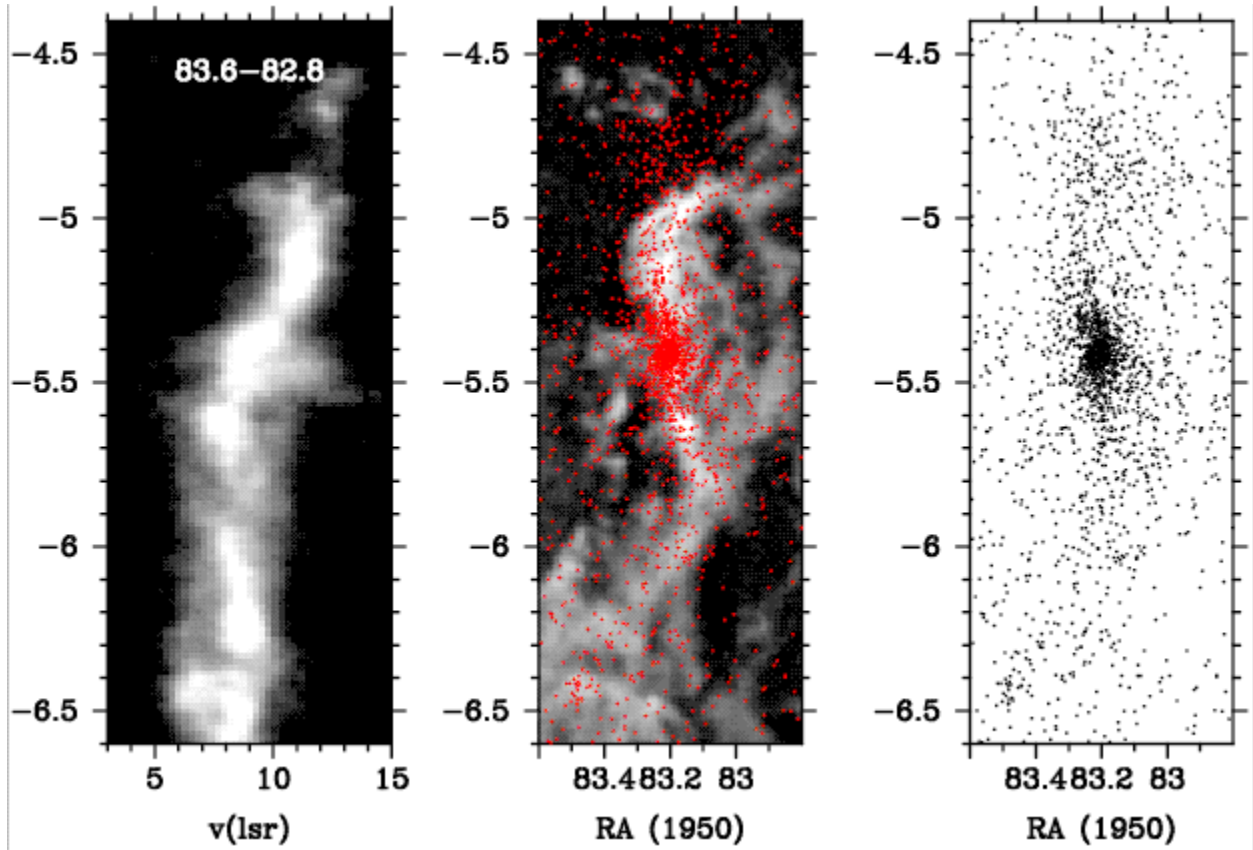


Fig. 2.— Spatial distribution of stars and gas in Orion A, compared with local kinematics. Left panel: ^{13}CO velocity-declination plot between RA = 83.6 and 82.8, taken from the data set of Bally et al. (1987). Right panel: distribution of near-infrared selected stars from Carpenter et al. (2001) (see text). Middle panel: superposition of stars onto the total ^{13}CO emission. .

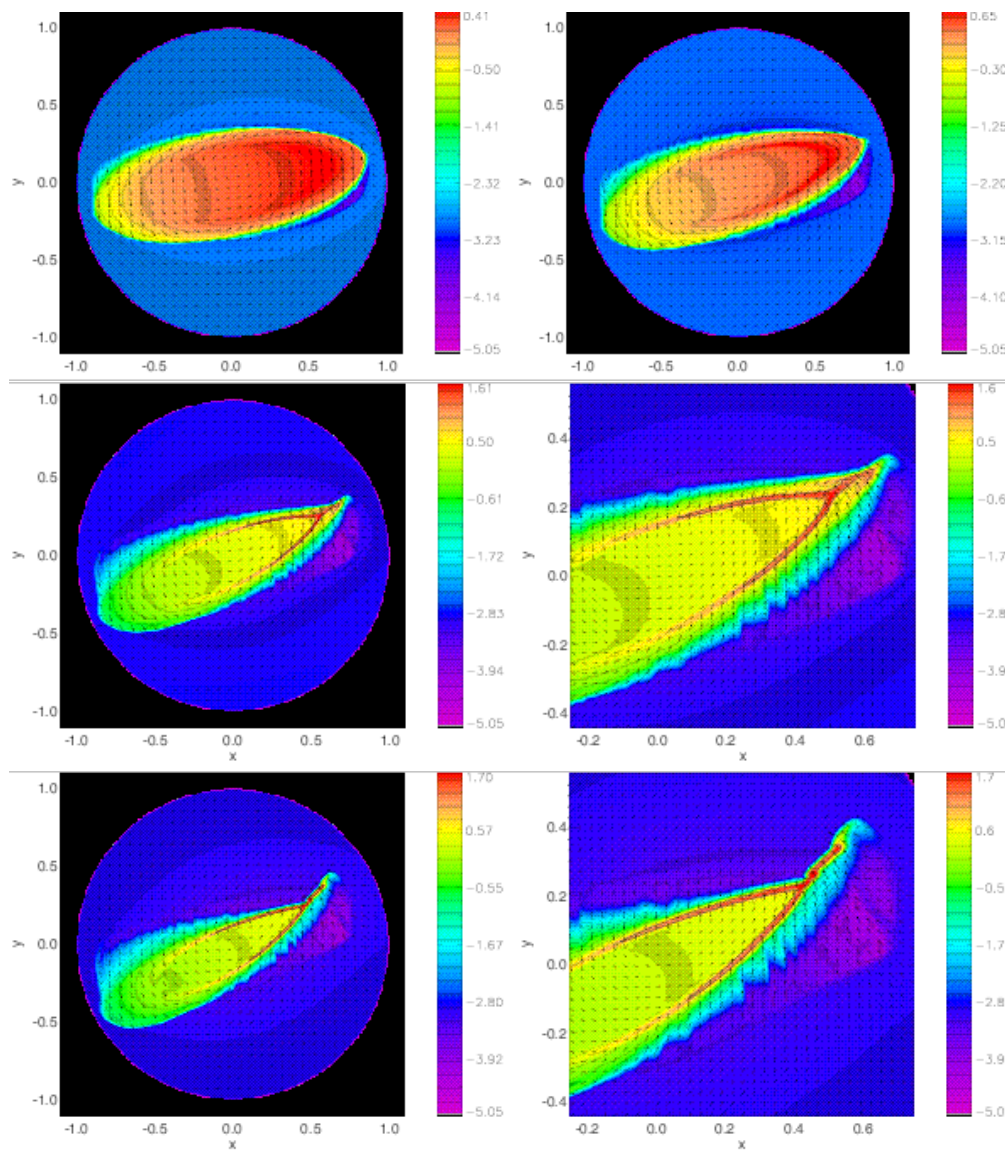


Fig. 3.— Collapse of the elliptical rotating sheet described in the text, showing the surface density distribution along with velocity vectors. The color bar indicates logarithmic values. A time sequence is shown in the upper left and upper right panels, followed by the middle left and lower left panels; the right middle and lower panels zoom in on the inner regions shown in the corresponding left middle and right panels. The snapshots correspond to times in code units of 0.075, 0.125, 0.175, and 0.209. The maximum velocity vector in each panel is 2.35, 2.82, 3.72, and 4.84 in code units, respectively, while the corresponding mass weighted velocities are 1.07, 1.2, 1.5, and 1.7. Note the formation of a V-shaped structure with a filament at the upper right.

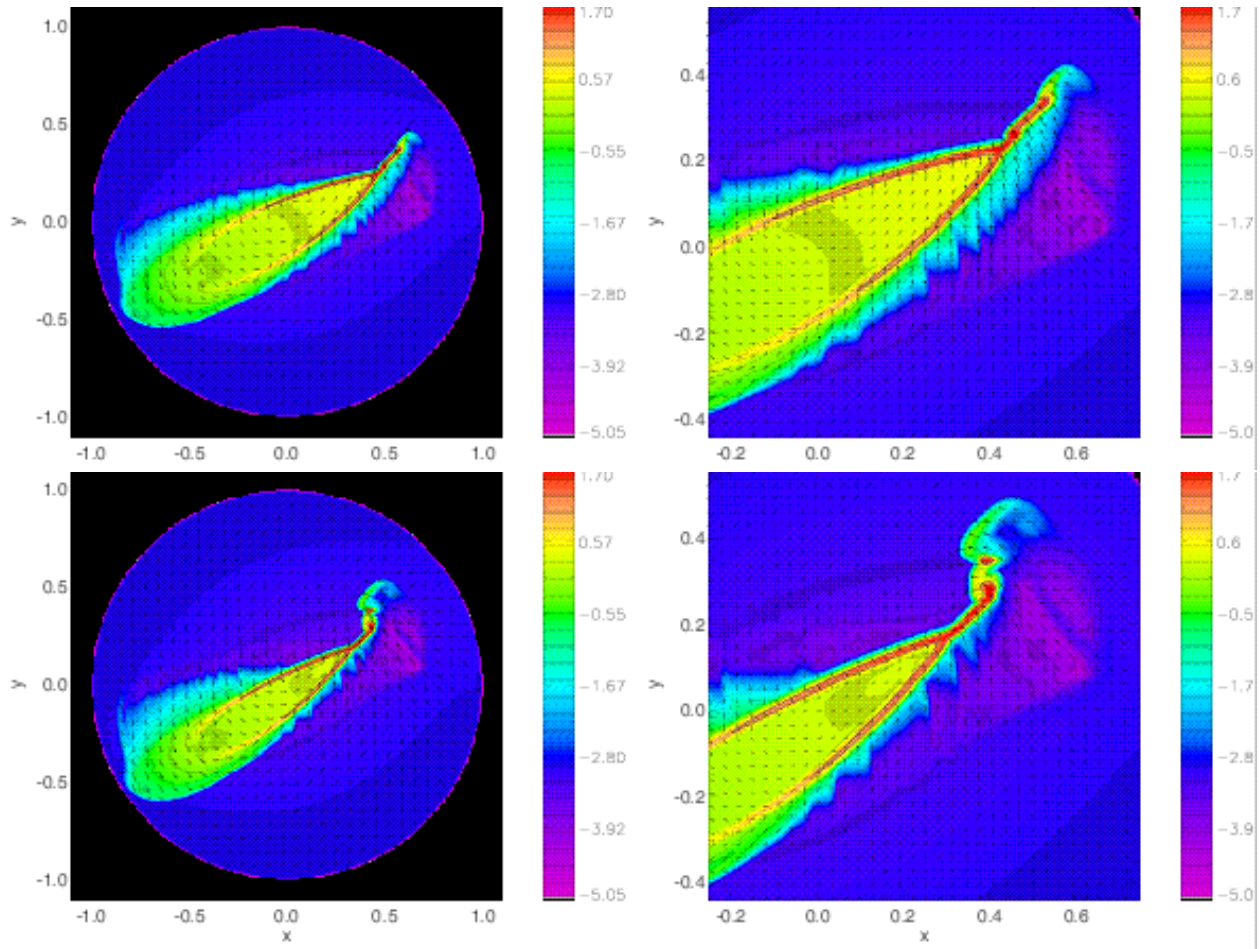


Fig. 4.— Final stages of evolution of the model in Figure 3, with the right-hand panels zooming in on the inner structure of the corresponding left-hand panels. The upper panels repeat the lower panels of Figure 3 at a time $t = 0.209$ for comparison with the final snapshot at $t = 0.25$. The final panels have maximum velocities of 10, with a mass-weighted velocity of 2.1 in code units. Note the development of something like the integral-shaped filament in the final stage, with denser concentrations that could represent the collection of protocluster gas (the details of these fragments are not reliable because of limited resolution).

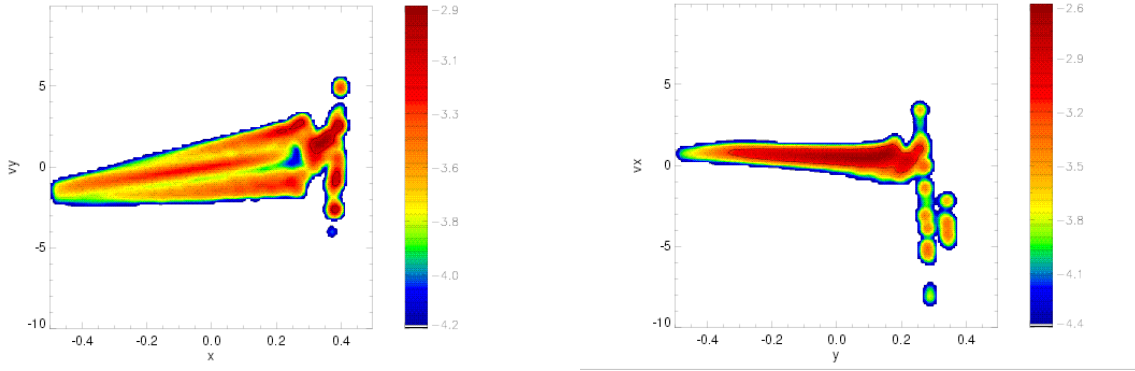


Fig. 5.— Mass-weighted position-velocity diagrams for the last snapshot of the model shown in Figure 4 (see text)

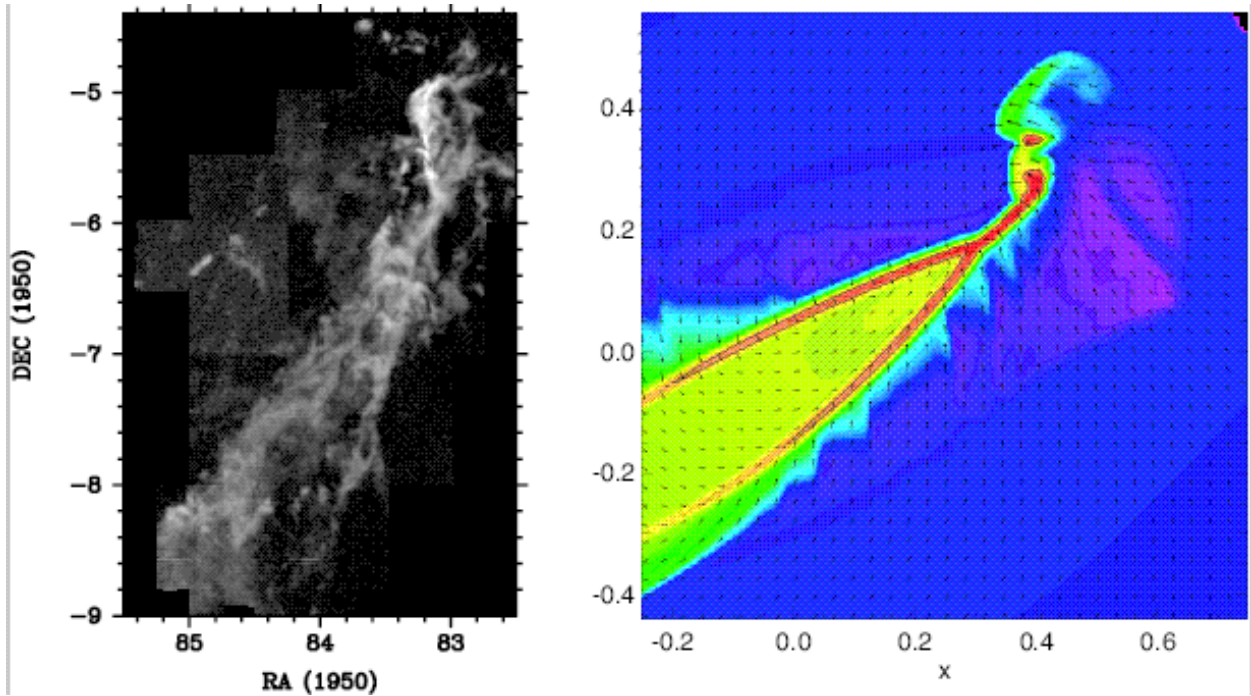


Fig. 6.— A side-by-side comparison of the ^{13}CO emission map from the left panel of Figure 1 with the final state of the model in the bottom right panel of Figure 4, using the scaling discussed in the text.